

# Insights into the Bimetallic Effects of a RhCo Catalyst for Ethene Hydroformylation: Experimental and DFT Investigations

Ning Huang, Boyang Liu, Xiaocheng Lan, and Tiefeng Wang\*



Cite This: *Ind. Eng. Chem. Res.* 2020, 59, 18771–18780



Read Online

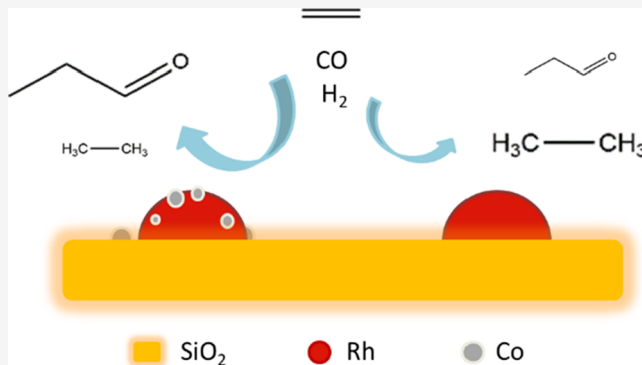
ACCESS |

Metrics & More

Article Recommendations

Supporting Information

**ABSTRACT:** Rh-based bimetallic catalysts are promising ligand-free heterogeneous catalysts for hydroformylation reactions. It is important to understand the mechanism of this bimetallic promotion for designing highly selective and active heterogeneous catalysts. In this work, the RhCo bimetallic catalyst was investigated focusing on the promotion effect of Co for the gas-phase hydroformylation of ethene. Adding Co to Rh increased both the catalytic productivity and selectivity to oxygenates. *In situ* diffuse reflectance infrared Fourier transform spectroscopy and CO-temperature programmed desorption were used to characterize CO adsorption. The results showed that the addition of Co to Rh changed the CO adsorption modes and strength for the Rh-based catalyst. Modulated CO adsorption strength was important to enhance selectivity. Density functional theory calculations were carried out to reveal the reaction mechanism. A reaction pathway was proposed to clarify the reason for enhanced selectivity on a RhCo bimetallic catalyst and show that the ratio between CO migration and desorption played a great role in this reaction.



## 1. INTRODUCTION

Hydroformylation is an industrial process with more than 10 million tons of products each year.<sup>1,2</sup> This process is a 100% atom effective reaction, and the desired oxygenate products are valuable chemicals in fine chemistry.<sup>3</sup> Hydroformylation is commonly conducted in a homogeneous system using Rh or Co complexes with phosphine ligands as catalysts.<sup>3–7</sup> Although this process has a high efficiency, it suffers from intrinsic industrial problems such as high operational pressure, difficult catalyst separation, noble metal loss, and solvent corrosivity.<sup>4,8</sup> Nowadays, several heterogeneous hydroformylation systems have been developed, such as immobilized homogeneous catalysts,<sup>9–11</sup> anchored Rh with phosphine-modified porous organic polymer catalysts,<sup>12–17</sup> supported ionic liquid-phase catalysts<sup>2,18</sup> and the use of water–oil biphasic catalytic processes.<sup>19–21</sup> Although these approaches can effectively separate the catalyst and products, they still need phosphine ligands, which are expensive, air and moisture sensitive, and tedious in work-up procedures.<sup>22,23</sup>

The development of ligand-free heterogeneous catalysts is important and environmentally benign for the hydroformylation reaction. In recent decades, the use of supported metal catalysts without ligands, which can be easily separated and avoid problems with phosphine, has gained much attention.<sup>4,24–30</sup> The main problem with metal catalysts is the low selectivity to oxygenate products caused by the hydrogenation and isomerization of alkene that occur as side reactions (**Scheme 1**). One way is to develop single-atom catalysts,

which can give high usage and a uniform electronic state of the active metal. The activity and selectivity can be improved on these catalysts.<sup>26,28–30</sup> Metal oxides, such as ZnO and CeO, have been chosen as effective supports for the hydroformylation reaction.<sup>28–31</sup> Until now, the choice of supports is limited, and the balance between the stability and activity of the catalyst is important.<sup>29</sup> Another way to improve the selectivity is using promoters, such as Co, Mo, V, and alkali metals.<sup>26,28–30,32–35</sup> Huang and Xu studied propylene hydroformylation catalyzed by Rh/SiO<sub>2</sub>. When Co was added, the selectivity to oxygenates was improved from 13 to 58%. The added Co influenced the electronic state of Rh and changed the reaction selectivity.<sup>36</sup> Ma *et al.* found that the addition of Co accelerated the conversion of dicyclopentadiene to diformyltricyclodecanes on Rh/Fe<sub>3</sub>O<sub>4</sub> when PPh<sub>3</sub> was used as the co-catalyst.<sup>35</sup> The increased dispersion and enhanced activity of the Rh catalyst were attributed to Co addition. In contrast, Navidi *et al.* found that the addition of Co decreased the conversion of ethene and selectivity to aldehydes.<sup>4</sup> These results show that it is still unclear how a second metal

Received: July 13, 2020

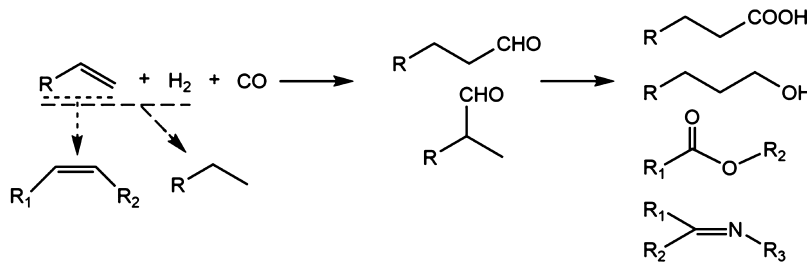
Revised: September 23, 2020

Accepted: September 25, 2020

Published: September 25, 2020



Scheme 1. Products from Hydroformylation and Related Side Reactions



influences the hydroformylation reaction, especially for cobalt that is extensively used in the hydroformylation process.

In this work, the promotion effect of Co on Rh active sites was investigated in the gas-phase hydroformylation of ethene. Transmission electron microscopy (TEM), CO chemisorption, hydrogen temperature-programmed reduction ( $H_2$ -TPR), *in situ* diffuse reflectance infrared Fourier transform spectroscopy (DRIFTS), and CO-temperature programmed desorption (CO-TPD) were used to characterize the catalysts and adsorption modes of CO. The reaction results indicated that adding Co to Rh increased both the catalytic activity and selectivity to oxygenates. A suitable CO adsorption was put forward to enhance the activity and selectivity for gas hydroformylation. The addition of Co suppressed the weak adsorption of CO and enhanced the activity of strongly adsorbed CO. Density functional theory (DFT) calculations were performed to suggest a reaction pathway on Rh(111) and RhCo(111) and a mechanism for different activities and selectivities of the two catalysts.

## 2. EXPERIMENTAL SECTION

**2.1. Materials.**  $SiO_2$  ( $S_{BET} = 140\text{ m}^2/\text{g}$ ) was purchased from Alfa Aesar (China) and crushed in 80–120 mesh.  $Co(NO_3)_2 \cdot 6H_2O$  (99%) and  $Rh(NO_3)_3$  (5% in aqueous  $HNO_3$ ) were purchased from Innochem (China). CO and  $C_2H_4$  gases were obtained from Air Liquid (China), and the other gases were provided by Beiwen (China).

**2.2. Catalyst Preparation.** The 0.6Rh0.23Co/SiO<sub>2</sub> bimetallic catalyst was prepared by incipient wetness co-impregnation with an aqueous solution of  $Co(NO_3)_2$  and  $Rh(NO_3)_3$  to give loadings of 0.6 wt % Rh and 0.23 wt % Co [ $Co/(Rh + Co) = 0.4$ , mol/mol]. After impregnation, the sample was treated in an ultrasonic bath for 2 h and then dried at 60 °C for 10 h, followed by calcination in air at 450 °C for 3 h. For comparison, 0.6 wt % Rh/SiO<sub>2</sub> and 1.0 wt % Co/SiO<sub>2</sub> monometallic catalysts were prepared by a similar method. Other  $xRhyCo/SiO_2$  bimetallic catalysts were prepared to study the effect of the Co/Rh ratio, where the loading of Rh was kept at 0.6 wt % and the amount of Co was increased from 0.11 to 3.09%. The notation of  $x$  and  $y$  represents the weight percentage of Rh and Co on SiO<sub>2</sub>, respectively.

**2.3. Catalyst Characterization.** TEM images were obtained on a JEM2010 TEM with a voltage of 120 kV. Before the measurement, the sample was reduced by 5%  $H_2$  in  $N_2$  (100 mL/min) for 30 min at 450 °C and then dispersed in alcohol. After an ultrasonic treatment for 30 min, the suspension was dropped onto a copper grid coated with carbon.

$H_2$ -TPR measurement was used to characterize the reduction properties of the catalysts using a ChemBET Pulsar TPR/TPD instrument (Quantachrome) equipped with a

thermal conductivity detector (TCD). For each test, 0.2 g of catalyst was loaded into a quartz U-tube and pretreated with flowing  $N_2$  at 200 °C for 1 h. After cooling to room temperature, the gas was changed to 5%  $H_2/Ar$  (100 mL/min) and kept flowing for 30 min to ensure a stable baseline signal. Then, the sample was heated to 800 °C at a rate of 10 °C/min.

CO chemisorption measurement was performed using the same apparatus as  $H_2$ -TPR to measure the number of metal active sites on the supported catalysts. 0.15 g of catalyst was first reduced by 5%  $H_2$  in Ar at 450 °C for 30 min, purged with flowing pure He at 450 °C for 30 min to remove adsorbed  $H_2$ , and then cooled to room temperature. Subsequently, CO/He pulses were injected consecutively until the detected size of the pulses became stable.

CO-TPD was performed to characterize the desorption temperature of CO on different catalysts. A mass spectrometer (MS, Pfeiffer Vacuum, Germany) was used to monitor CO and  $CO_2$  desorbed from the catalyst. 0.2 g of catalyst was reduced in 1%  $H_2$  balanced with Ar (100 mL/min) at 450 °C for 1 h, cooled to room temperature, and exposed to 10% CO balanced with He for 30 min. The sample was purged by Ar (100 mL/min) for 30 min to remove physically adsorbed gas. Then, the temperature was increased to 450 °C at a rate of 10 °C/min for CO-TPD measurement.

*In situ* DRIFTS was performed using a Nicolet 6700 spectrometer (Thermo Fisher Scientific) equipped with a PIKE reaction chamber. The sample was pretreated in 1%  $H_2$  balanced with Ar at 450 °C for 30 min and then cooled to 40 °C for adsorption. CO adsorption was performed with a flow of 1000 ppm CO diluted in  $N_2$  for 60 min. Then, the sample was purged with  $N_2$  flow for 30 min and heated to 350 °C at a rate of 10 °C/min. Spectra were collected at a resolution of 4  $cm^{-1}$ .

**2.4. Catalytic Evaluation.** The gas-phase reaction of ethene hydroformylation was carried out in a fixed bed continuous flow reactor (ID 7.5 mm) with a quartz tube (ID 5.5 mm) inside. The catalyst (0.2 g) was loaded in the middle of the tube to ensure a uniform temperature for the catalyst bed (length was 15 mm), which was fixed in a position by quartz sand below. The catalyst was first reduced in 15%  $H_2/N_2$  at 450 °C for 30 min. After cooling to a specific temperature, the catalyst was exposed to the reaction gas and the total pressure was increased to 1 MPa. The reaction temperature was 180 °C, and the total gas flow rate was 20  $cm^3/\text{min STP}$  ( $C_2H_4/CO/H_2/N_2$  of 1:1:1:1) unless specified otherwise.

The products were analyzed online using a GC7890B gas chromatograph (Agilent, US). Aldehydes and alcohols were separated by a capillary column (Agilent, HP-INNOWax) connected to a flame ionization detector, and other products were separated by packed columns (Agilent, Molsieve 5A and

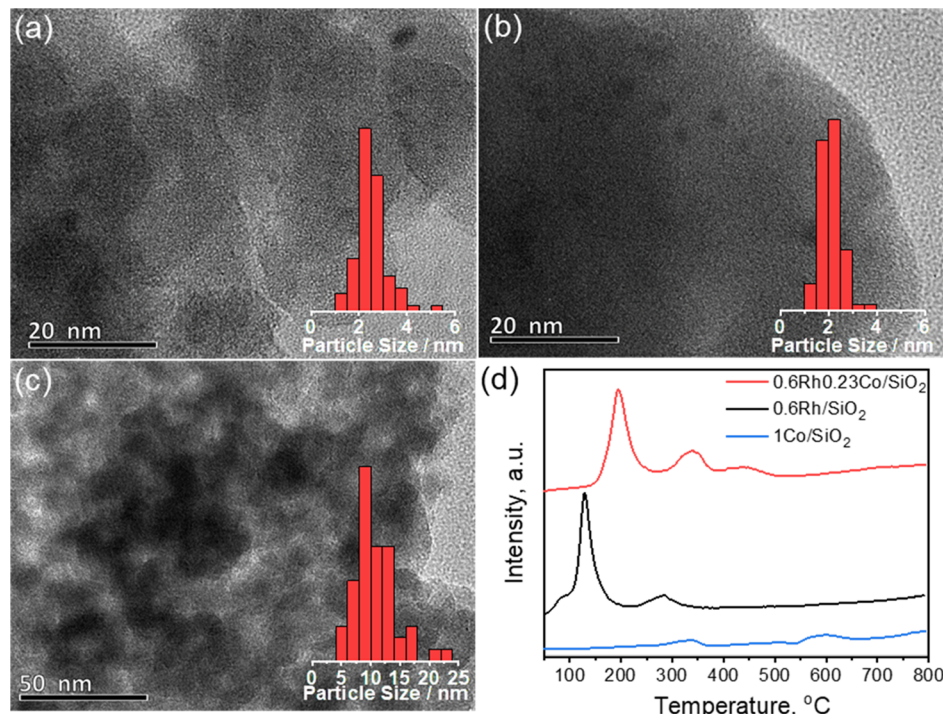


**Figure 1.** TEM images and metal particle size distributions of (a) 0.6Rh/SiO<sub>2</sub>, (b) 0.6Rh0.23Co/SiO<sub>2</sub>, and (c) 1Co/SiO<sub>2</sub>; (d) H<sub>2</sub>-TPR profiles of 0.6Rh/SiO<sub>2</sub>, 1Co/SiO<sub>2</sub>, and 0.6Rh0.23Co/SiO<sub>2</sub>.

HayeSep N 80) and detected with a TCD. The catalytic productivity, turn over frequency (TOF), and selectivity for each product were calculated by the following equations

$$\text{Productivity}_i (\text{mol} \cdot \text{mol}_{\text{Rh}}^{-1} \cdot \text{h}^{-1}) = \frac{n_i F_i}{m_{\text{Rh}} / M_{\text{Rh}}}$$

$$\text{TOF}_i (\text{h}^{-1}) = \frac{n_i F_i}{n_{\text{active sites}}}$$

$$\text{Selectivity}_i (\%) = \frac{n_i F_i}{\sum n_i F_i} \times 100$$

where  $n_i$  is the number of ethene molecules in product  $i$ ,  $F_i$  is the molar flow rate of product  $i$ ,  $m_{\text{Rh}}$  is the mass of Rh used for the reaction,  $M_{\text{Rh}}$  is the relative atomic mass of Rh, and  $n_{\text{active sites}}$  is the total active sites of the catalyst measured by CO chemisorption.

**2.5. Computational Method.** DFT calculations by the Vienna ab initio simulation package were used to understand the reaction mechanism on Rh(111) and Rh<sub>1</sub>Co<sub>1</sub>(111).<sup>37,38</sup> The metal surface was modeled with a three-layer slab separated by 15 Å of vacuum. The supercell size was 2 × 2. The Perdew–Burke–Ernzerhof function was used to calculate the exchange–correlation interaction.<sup>39</sup> 3 × 3 × 1  $k$ -point sampling was used, and the energy cutoff was 400 eV. Transition states (TSs) were searched by the climbing-image nudged elastic band method<sup>40</sup> and were further calculated using the dimer method.<sup>41–43</sup> The number of images was six, and all TSs were confirmed by vibrational analysis.

### 3. RESULTS AND DISCUSSION

**3.1. Catalyst Characterization.** The morphology of all catalysts was observed by TEM. Representative images are shown in Figure 1. The particle size distribution of each

catalyst was determined by measuring more than 100 particles. For the 0.6Rh/SiO<sub>2</sub> catalyst, the metal particles were 1–6 nm with a mean size of 2.5 nm. The addition of Co slightly decreased the mean particle size to 2.1 nm, while the size distribution was almost the same as that of 0.6Rh/SiO<sub>2</sub>. However, the metal particles of 1Co/SiO<sub>2</sub> were much larger than those of 0.6Rh/SiO<sub>2</sub> and 0.6Rh0.23Co/SiO<sub>2</sub>, with a mean size of 11 nm. The number of metal active sites was estimated by CO chemisorption. The data are summarized in Table S1. The CO uptake was 1.04 μmol/g<sub>cat</sub> for 0.6Rh/SiO<sub>2</sub> and 0.12 μmol/g<sub>cat</sub> for Co/SiO<sub>2</sub>, and it increased to 1.68 μmol/g<sub>cat</sub> for 0.6Rh0.23Co/SiO<sub>2</sub>. The TEM images (Figure 1a,b) showed that the addition of Co to the Rh catalyst did not increase the size of the metal nanoparticles; therefore, Co should be incorporated into the nanoparticles and increase the dispersion of Rh, leading to higher CO uptake value for 0.6Rh0.23Co/SiO<sub>2</sub>.

To investigate the interaction between Rh and Co, H<sub>2</sub>-TPR was used to characterize the reducibility of the metal of 0.6Rh/SiO<sub>2</sub>, 0.6Rh0.23Co/SiO<sub>2</sub>, and 1Co/SiO<sub>2</sub>. As shown in Figure 1d, there were three H<sub>2</sub> reduction peaks in the TPR profile of 0.6Rh/SiO<sub>2</sub>: the main peak at 130 °C, its shoulder peak at 85 °C, and the peak at 280 °C. In the TPR profile of 0.6Rh/SiO<sub>2</sub> in this work, the shoulder peak at 85 °C and the main peak at 130 °C were assigned to the rapid reduction of surface Rh and slower reduction of bulk Rh atoms, respectively. The peak at 280 °C was assigned to the reduction of Rh<sub>2</sub>O<sub>3</sub> interacting with the support.<sup>44</sup> For the 1Co/SiO<sub>2</sub> catalyst, two peaks were observed in the TPR profile. The first peak occurred at 280–380 °C and the second one at 540–650 °C, in agreement with the previous results.<sup>45,46</sup> The first peak was assigned as the reduction of Co<sub>3</sub>O<sub>4</sub> to Co<sup>0</sup> via CoO, and the second one was assigned to the reduction of surface cobalt hydroxy silicates.<sup>45</sup>

The 0.6Rh0.23Co/SiO<sub>2</sub> bimetallic catalyst exhibited peak shifts compared with both Rh and Co monometallic catalysts.

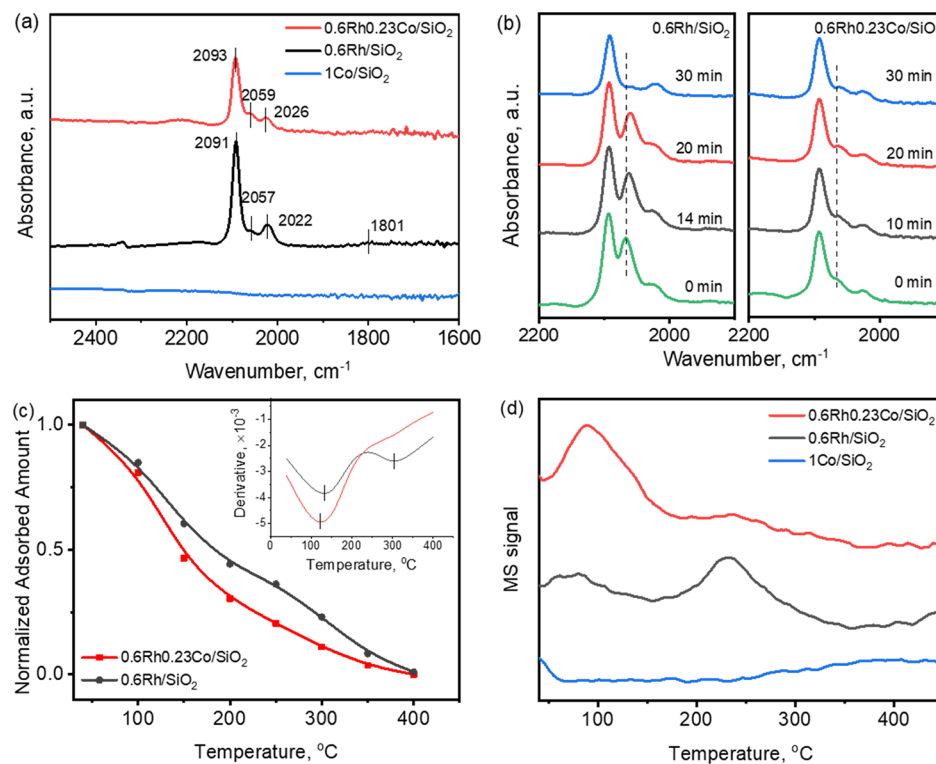


**Figure 2.** Related CO interactions with 0.6Rh/SiO<sub>2</sub>, 1Co/SiO<sub>2</sub>, and 0.6Rh0.23Co/SiO<sub>2</sub>. (a,b) DRIFTS of CO adsorption at 40 °C: spectra collected after CO adsorption for 60 min and then N<sub>2</sub> purging for 30 min (a), and time-related spectra during N<sub>2</sub> purging (b); (c) normalized residual amount of CO on catalysts determined by DRIFTS and the first derivative of the adsorbed amount curves; (d) CO-TPD profiles.

The Rh reduction peaks shifted to higher temperatures while those of the Co species shifted to lower temperatures. As shown in Figure 1d, 0.6Rh0.23Co/SiO<sub>2</sub> showed three peaks: the first peak at 200 °C was ascribed to the reduction of Rh<sub>2</sub>O<sub>3</sub>, which shifted from the main peak accompanied by its shoulder peak for 0.6Rh/SiO<sub>2</sub>; the second peak at 280–390 °C was ascribed to the reduction of both Rh and Co species; and the last peak at 400–510 °C was from the reduction of surface hydroxy silicates of cobalt. The addition of Co made the reduction of Rh more difficult, and the spillover of activated hydrogen from reduced Rh facilitated the reduction of Co. Although 0.6Rh0.23Co/SiO<sub>2</sub> was more difficult to reduce than 0.6Rh/SiO<sub>2</sub>, both catalysts could be reduced below 450 °C, which confirmed that all the catalysts were reduced before the hydroformylation reaction.

**3.2. CO Interaction with the Catalyst Surface.** The 0.6Rh/SiO<sub>2</sub>, 1Co/SiO<sub>2</sub>, and 0.6Rh0.23Co/SiO<sub>2</sub> catalysts were further characterized by *in situ* DRIFTS of adsorbed CO. The adsorption states are shown in Figure 2a. The 1Co/SiO<sub>2</sub> catalyst showed no CO adsorption during the whole operation, which was consistent with its very low CO uptake. After sweeping the weakly adsorbed CO, the 0.6Rh/SiO<sub>2</sub> catalyst showed four peaks, which belonged to three CO adsorption states on Rh. The two peaks at 2091 and 2022 cm<sup>-1</sup> were ascribed to the symmetric and asymmetric stretches of Rh(CO)<sub>2</sub> *gem*-dicarbonyl species, respectively. The peak at 2057 cm<sup>-1</sup> was attributed to linearly adsorbed CO, and the broad peaks at 1801 cm<sup>-1</sup> was ascribed to bridge adsorbed CO.<sup>47</sup> The spectra of adsorbed CO on 0.6Rh0.23Co/SiO<sub>2</sub> only showed the Rh(CO)<sub>2</sub> *gem*-dicarbonyl (2093 and 2026 cm<sup>-1</sup>) and linear Rh–CO (2059 cm<sup>-1</sup>) species. Although the bridge adsorbed CO is usually found over supported metal catalysts, it was not observed here. Tomishige *et al.* studied CO

adsorption on a Rh–Mo catalyst and also found that the amount of bridging CO was negligible and twin CO was dominant.<sup>32</sup> This phenomenon was probably due to high dispersion of the Rh species and low concentration of bridge adsorbed CO. The band positions for 0.6Rh0.23Co/SiO<sub>2</sub> slightly blue-shifted compared to those of the 0.6Rh/SiO<sub>2</sub> catalyst. It may be caused by electron deficiency of Rh with the addition of Co, which was beneficial for hydroformylation selectivity.<sup>8,26</sup>

After changing the gas atmosphere to pure nitrogen, the intensities for Rh(CO)<sub>2</sub> *gem*-dicarbonyl species were almost unchanged over 0.6Rh/SiO<sub>2</sub>, but there was a remarkable decrease of intensity for the linear Rh–CO band (2057 cm<sup>-1</sup>) (Figure 2b). This observation suggested that the active sites for the linear Rh–CO species on 0.6Rh/SiO<sub>2</sub> only had a weak interaction with CO. On the contrary, there were no such sites for weakly adsorbed linear Rh–CO species on 0.6Rh0.23Co/SiO<sub>2</sub>. Similar intensity change for linear adsorbed CO was also observed on Rh confined within the silicate-1 catalyst (Rh@S-1).<sup>27</sup> These results indicated that 0.6Rh/SiO<sub>2</sub> contained a high proportion of Rh sites that only weakly adsorbed CO and after adding Co, these sites were mostly suppressed.

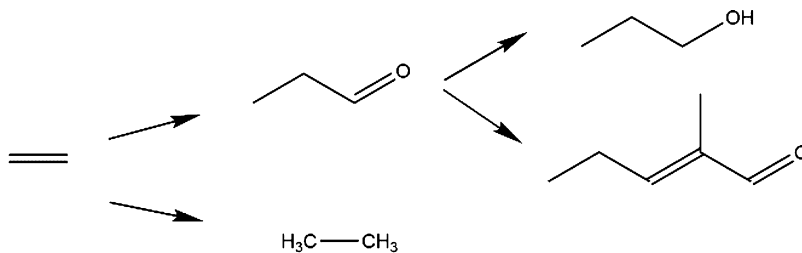
For the heterogeneous hydroformylation reaction, the adsorption and subsequent insertion of CO are considered to be the key steps.<sup>24</sup> The CO adsorption amount of the catalysts followed the trend of 0.6Rh0.23Co/SiO<sub>2</sub> > 0.6Rh/SiO<sub>2</sub> > 1Co/SiO<sub>2</sub>, as shown by the CO chemisorption results (Table S1). CO desorption at different temperatures was also studied by DRIFT (Figures S1 and 2c) to characterize its adsorption strength. At 350 °C, there were almost no CO left on the 0.6Rh0.23Co/SiO<sub>2</sub> surface (Figure S1b). However, it was more difficult to desorb CO from 0.6Rh/SiO<sub>2</sub>, and some Rh(CO)<sub>2</sub> *gem*-dicarbonyl species still remained at 350 °C

Table 1. Catalytic Performance of the Rh-Based Catalysts<sup>a</sup>

catalyst	productivity, mol/(mol <sub>Rh</sub> ·h)	TOF (h <sup>-1</sup> )	selectivity (%)				
			ethane	propanal	1-propanol	2M2P	oxy.
0.6Rh/SiO <sub>2</sub>	42	2511	57	38	1	4	43
0.6Rh0.23Co/SiO <sub>2</sub>	75	2790	48	46	0.7	5	52
0.6Rh + 0.23Co	29		57	40	0.4	2	43

<sup>a</sup>Reaction conditions:  $T = 180\text{ }^{\circ}\text{C}$ ,  $P = 1\text{ MPa}$ , GHSV = 6000 mL/(g<sub>cat</sub>·h), H<sub>2</sub>/CO/C<sub>2</sub>H<sub>4</sub>/N<sub>2</sub> = 1:1:1:1; 2M2P: 2-methyl-2-pentenal, oxy.: oxygenates.

Scheme 2. Hydroformylation and Hydrogenation Reaction Pathways of Ethene



(Figure S1a). Considering the adsorption amount of CO at 40 °C as the total adsorbed CO on each catalyst, the normalized amounts of residual CO at different temperatures were determined by the corresponding peak areas (Figure 2c). This value on 0.6Rh0.23Co/SiO<sub>2</sub> was lower than that on 0.6Rh/SiO<sub>2</sub> in the low temperature range. The first derivative of the CO residue curve inserted in Figure 2c further showed the relative amount of desorbed CO at each temperature, with one broad peak for 0.6Rh0.23Co/SiO<sub>2</sub> and two obvious peaks for 0.6Rh/SiO<sub>2</sub>. These results showed that CO mainly desorbed from 0.6Rh0.23Co/SiO<sub>2</sub> at low temperatures but a fraction of CO desorbed from 0.6Rh/SiO<sub>2</sub> at higher temperatures. At the reaction temperature, 180 °C, nearly half of CO was desorbed; thus, there were enough vacant active sites for ethene and H atoms.

CO-TPD was used to further compare the adsorption strength of CO, as shown in Figure 2d. For 1Co/SiO<sub>2</sub>, no CO desorbed below 200 °C and a small desorption peak appeared in the range of 300–450 °C, confirming that CO was difficult to be adsorbed on this Co/SiO<sub>2</sub> surface. Zhao *et al.* reported that there was no obvious CO desorption from a Co-based catalyst in the range of 100–300 °C because CO was dissociated on cobalt.<sup>48</sup> 0.6Rh/SiO<sub>2</sub> gave two desorption peaks of CO at 70 and 230 °C. Tomishige *et al.* also reported two peaks below 320 °C.<sup>32</sup> The 0.6Rh0.23Co/SiO<sub>2</sub> catalyst gave a similar curve to 0.6Rh/SiO<sub>2</sub> but with differences in some details. 0.6Rh0.23Co/SiO<sub>2</sub> also gave two CO desorption peaks, but the first peak had higher intensity than the latter at 237 °C, which is consistent with the CO residual analysis in Figure 2c. Meanwhile, the peak temperature in CO-TPD for 0.6Rh0.23Co/SiO<sub>2</sub> shifted from 70 to 90 °C, compared with 0.6Rh/SiO<sub>2</sub>. These results suggested that Co addition modified the active sites of the Rh catalyst to increase the ratio of CO adsorbed in the low temperature range with a slight increase in the adsorption strength. *In situ* DRIFTS showed the weakly adsorbed linear CO species on 0.6Rh/SiO<sub>2</sub>. Here, the CO-TPD results further showed that a part of CO had weaker adsorption on 0.6Rh/SiO<sub>2</sub>, which desorbed at 70 °C, than on RhCo/SiO<sub>2</sub>. We would speculate that this kind of site has little contribution to hydroformylation but is responsible for hydrogenation because they can hardly adsorb CO at the reaction temperature.

**3.3. Catalytic Evaluation.** The catalytic performance was evaluated for the hydroformylation of ethene. The results are listed in Table 1 and Figure S2. On the Rh/SiO<sub>2</sub> and RhCo/SiO<sub>2</sub> catalysts, four products were produced through two pathways (Scheme 2): propanal, 1-propanol, and 2-methyl-2-pentenal were produced from hydroformylation, while ethane was produced from hydrogenation. At the experimental conditions, the Co/SiO<sub>2</sub> catalyst showed no activity.

For 0.6Rh/SiO<sub>2</sub>, the catalyst productivity was 44 mol/(mol<sub>Rh</sub>·h) and the TOF was 2511 h<sup>-1</sup> at the time on stream (TOS) of 5 h. The propanal selectivity was 38%, and the total selectivity to oxygenates was 43%. The detailed product distribution is summarized in Table 1. The 0.6Rh0.23Co/SiO<sub>2</sub> catalyst was then studied. A physically mixed catalyst (0.6Rh + 0.23Co) containing the same metal content as 0.6Rh0.23Co/SiO<sub>2</sub> was also evaluated for comparison. As listed in Table 1, the catalytic performance of 0.6Rh + 0.23Co was very similar to that of 0.6Rh/SiO<sub>2</sub>, indicating that the 0.6Rh/SiO<sub>2</sub> and 1Co/SiO<sub>2</sub> catalysts worked independently in the physically mixed catalyst considering that 1Co/SiO<sub>2</sub> was almost inert for this reaction. In contrast, the 0.6Rh0.23Co/SiO<sub>2</sub> bimetallic catalysts gave 75 mol/(mol<sub>Rh</sub>·h) productivity and 46% propanal selectivity. The catalyst productivity was much higher than that of 0.6Rh/SiO<sub>2</sub>, and the selectivity was also enhanced. During the evaluation time, the catalyst performance was kept stable (Figure S3). The change in the Rh and Co contents was negligible based on inductively coupled plasma atomic emission spectroscopy. However, the leaching of the metal may become significant in a liquid reaction system.<sup>49</sup>

As CO played an important role in hydroformylation,<sup>24</sup> the influence of the CO/H<sub>2</sub> ratio was also studied (Figure S4). When the CO/H<sub>2</sub> ratio increased from 1:2 to 2:1, the selectivity to oxygenates increased from 48 to 63%, but the productivity decreased from 98 to 46 mol/(mol<sub>Rh</sub>·h). For homogeneous hydroformylation reaction, according to the commonly accepted mechanism, the catalyst needs to first eliminate one CO ligand from each Rh site for the next step to occur and excess CO will lead to a poisoned state.<sup>50</sup> From a similar point of view in heterogeneous catalysis, the surface concentrations of C<sub>2</sub>H<sub>4</sub> and H<sub>2</sub> decrease at higher CO concentration because CO is the most abundant surface

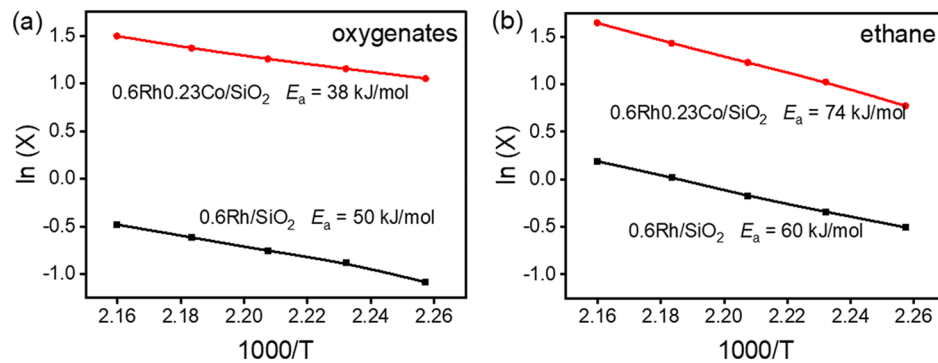


**Figure 3.** Apparent activation energy for formation of oxygenates (a) and ethane (b) over 0.6Rh/SiO<sub>2</sub> and 0.6Rh0.23Co/SiO<sub>2</sub>. Reaction conditions:  $P = 1 \text{ MPa}$ , GHSV = 9000 mL/(g<sub>cat</sub>·h), H<sub>2</sub>/CO/C<sub>2</sub>H<sub>4</sub> = 1:1:1.

species.<sup>4,26</sup> This decrease in reactant concentrations decreased the catalyst productivity.

The activity was influenced by the amount of active sites and the bimetallic interaction on the catalyst surface. The CO uptake results (Table S1) showed that the 0.6Rh0.23Co/SiO<sub>2</sub> catalyst had higher CO uptake than the 0.6Rh/SiO<sub>2</sub> catalyst, which partly explained the enhanced activity of 0.6Rh0.23Co/SiO<sub>2</sub>. For the 1Co/SiO<sub>2</sub> catalyst, CO was hardly adsorbed on the catalyst thus, the activity of 1Co/SiO<sub>2</sub> is negligible, and Co acts as a promoter in the RhCo bimetallic catalyst. Furthermore, TOF comparison (Table 1) showed that each active site on 0.6Rh0.23Co/SiO<sub>2</sub> had higher activity than on the 0.6Rh/SiO<sub>2</sub> catalyst. This further increases the total activity of 0.6Rh0.23Co/SiO<sub>2</sub>. CO adsorption and desorption behaviors are important for the selectivity to oxygenates in the hydroformylation reaction. The CO desorption profiles from DRIFTS and CO-TPD results confirmed that the addition of Co significantly affected CO desorption from Rh (Figure 2c,d). CO exhibited a two-step desorption from 0.6Rh/SiO<sub>2</sub>, while the first desorption step dominated the CO desorption from 0.6Rh0.23Co/SiO<sub>2</sub>. The decreased desorption temperature indicated that CO adsorbed on 0.6Rh0.23Co/SiO<sub>2</sub> had a suitable adsorption state, which favored migration and insertion into adsorbed ethyl compared to 0.6Rh/SiO<sub>2</sub>.<sup>8,27</sup> As the insertion of CO into adsorbed ethyl is a crucial step of hydroformylation, the production of propanal is enhanced and the formation of ethane is inhibited by this facile CO insertion. Meanwhile, the sites on 0.6Rh/SiO<sub>2</sub> that weakly adsorb CO favor hydrogenation and decrease the selectivity to oxygenates.

The apparent activation energy ( $E_a$ ) over the bimetallic and monometallic catalysts was measured to further clarify the Co promotion effect. The experiments were carried out at conditions where the influence of external diffusion was excluded (Figure S5) and the conversion was controlled below 10%. The influence of temperature on hydroformylation and hydrogenation over 0.6Rh0.23Co/SiO<sub>2</sub> and 0.6Rh/SiO<sub>2</sub> is shown in Figure 3. Using the Arrhenius equation, the apparent activation energies for the formation of both ethane and oxygenates were calculated. In the temperature range of 170–190 °C, both catalysts showed higher  $E_a$  for ethane than oxygenate production, in agreement with the previous measurements (Table S2).<sup>4,32</sup> The energy barrier of oxygenates was lower than that of ethane formation; thus, the formation of ethane was more sensitive to temperature, and the selectivity to oxygenates decreased with increasing temperature (57 and 46% at 170 and 190 °C on 0.6Rh0.23Co/SiO<sub>2</sub>, respectively). It is important to note that compared with 0.6Rh/SiO<sub>2</sub>,

0.6Rh0.23Co/SiO<sub>2</sub> increased  $E_a$  for ethane production by 14 kJ/mol and decreased  $E_a$  for oxygenate productions by 12 kJ/mol. This change in activation energy indicated the change of catalysts and improved the hydroformylation activity and oxygenate selectivity over 0.6Rh0.23Co/SiO<sub>2</sub>.

The RhCo/SiO<sub>2</sub> bimetallic catalysts with different Co/Rh ratios were evaluated at a fixed Rh loading of 0.6 wt %. The results are shown in Figure 4. The addition of Co increased the

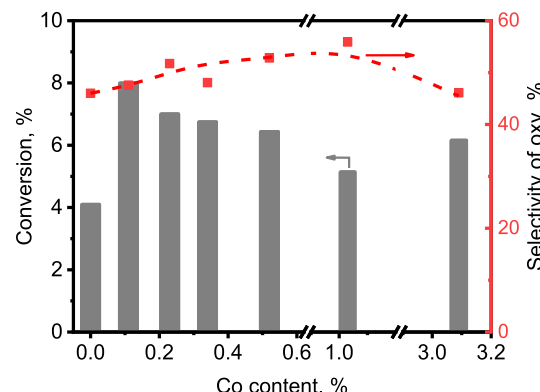


**Figure 4.** Catalytic performance of RhCo/SiO<sub>2</sub> bimetallic catalysts with different Co contents. Reaction conditions:  $T = 180 \text{ }^\circ\text{C}$ ,  $P = 1 \text{ MPa}$ , GHSV = 6000 mL/(g<sub>cat</sub>·h), H<sub>2</sub>/CO/C<sub>2</sub>H<sub>4</sub>/N<sub>2</sub> = 1:1:1:1, TOS = 5 h.

catalytic productivity and oxygenate selectivity. The highest activity was obtained at 0.6Rh0.11Co/SiO<sub>2</sub>, giving 86 mol/(mol<sub>Rh</sub>·h) catalytic productivity. Further addition of Co slightly decreased the catalytic activity, but the productivity was still higher than that over 0.6Rh/SiO<sub>2</sub>. With the increased addition of Co, the selectivity to oxygenates increased from 46% over 0.6Rh/SiO<sub>2</sub> to 48% over 0.6Rh0.11Co/SiO<sub>2</sub> and then reached the highest oxygenate selectivity of 56% over 0.6Rh0.03Co/SiO<sub>2</sub>. With further addition of Co, the selectivity decreased to 46% over 0.6Rh3.09Co/SiO<sub>2</sub>. The catalytic performance was compared with other reported supported catalyst without phosphine ligands in gas-phase hydroformylation of ethene, as listed in Table S3. For heterogeneous ethene hydroformylation reaction, higher pressure enhanced activity and slightly increased oxygenate selectivity.<sup>4</sup> Higher temperature also enhanced catalyst activity but decreased the oxygenate selectivity.<sup>4,25</sup> The Rh metal was the most common catalyst, and several promoters have been tried to improve its selectivity. The current RhCo/SiO<sub>2</sub> catalyst improved the selectivity of oxygenates, giving an upper-middle level of

selectivity and reached the highest oxygenate productivity among the recent research studies.

**3.4. DFT Calculations.** DFT calculations were carried out to understand the reaction pathways on Rh(111) and RhCo(111) (Figure S6). The adsorption geometries and binding energies were studied for all reactants. On Rh(111), CO preferred to adsorb on the hollow site ( $-2.20$  eV), which was  $\sim 0.2$  eV more stable than the top site ( $-2.02$  eV) and bridge site ( $-1.97$  eV). Similarly, H adsorption was more stable on the hollow site ( $-0.59$  eV) than on the top ( $-0.22$  eV) and bridge ( $-0.49$  eV) sites at 1/4 ML coverage. Ethene adsorption was more complicated, and the  $\pi$  mode ( $-1.44$  eV) was preferred, which was consistent with previous calculations.<sup>51,52</sup> The thickness of the metal slab in the model was also considered using CO adsorption on the Rh(111) surface. A thicker slab slightly decreased the adsorption energy of CO, but the trend at various sites was consistent, as shown in Figure S7. To save the computational cost, a three-thick slab was used for further study.

It has been proposed in the previous studies that hydroformylation needs three steps: (I) ethene hydrogenates to ethyl, (II) CO inserts between adsorbed ethyl and the active site, and (III) adsorbed propionyl hydrogenates to propanal.<sup>4,26</sup> Herein, a similar mechanism was used in DFT calculations to verify the reaction route and investigate the factors affecting the hydroformylation and hydrogenation selectivities. The related reaction states on Rh(111) are shown in Figure 5. H was adsorbed on a vacant hollow site adjacent to  $\pi$ -adsorbed ethene. The adsorbed H attacked ethene along the C=C double bond to form ethyl with an energy barrier of 0.47 eV. CO then migrated to the ethyl flank and inserted itself between the ethyl and Rh with an activation energy of 0.91 eV. The formed propionyl was adsorbed with C

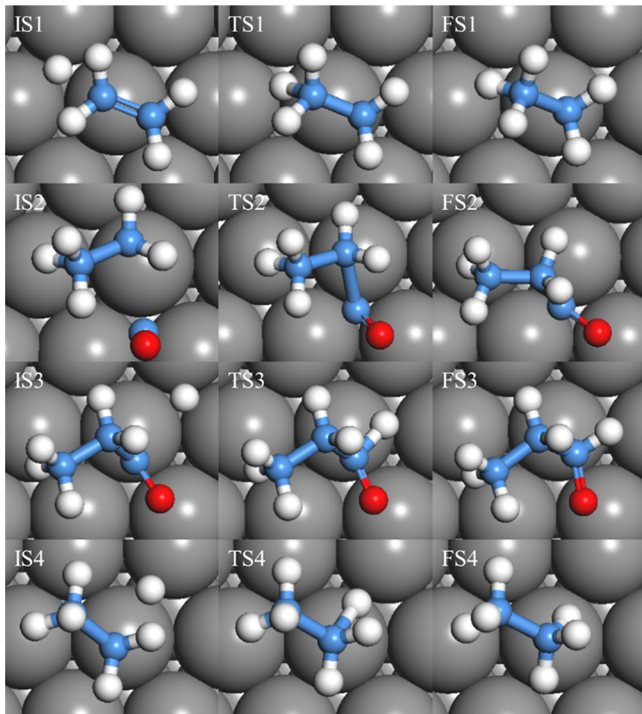


**Figure 5.** Initial states (IS), TS, and final states of the hydroformylation reaction on the Rh(111) surface. Rh, C, O, and H atoms are grey, blue, red and white, respectively.

on the bridge site and O atop Rh. For further hydrogenation, propionyl moved to form a di- $\sigma$  geometry and an adsorbed H attacked the carbonyl C to form propanal. The activation energy of TS3 was 0.61 eV. This route produced aldehyde. However, ethyl can also be hydrogenated through TS4 to produce the byproduct ethane. Although the energy barrier of TS4 was relatively low (0.28 eV), the previous step, which was the replacement of CO with H, was highly endothermic (1.38 eV). A similar reaction pathway can be proposed on RhCo(111), as shown in Figure S8. Differences were found with TS2 and TS4. Unlike on the Rh(111) surface, the produced propionyl after CO insertion was adsorbed in the di- $\sigma$  mode on RhCo(111) with carbonyl C and O bonded on Rh and Co, respectively. This geometry led to a more stable adsorption. The second difference was with ethyl hydrogenation to ethane. Instead of the bridge adsorbed H on the Rh(111) surface, H adsorbed on a Rh–Rh–Co hollow site attacked ethyl on the RhCo(111) surface.

Figure 6 shows the energy profiles that accounted for the promotion by Co. In the pathway of ethene hydroformylation

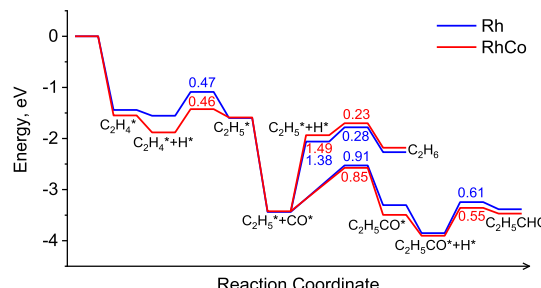


**Figure 6.** Hydroformylation reaction pathways on Rh(111) and RhCo(111) surfaces. The reaction states are labeled, and “\*” denotes an adsorbed state. The energy barrier on Rh and RhCo is marked in blue and red, respectively.

to propanal on the Rh(111) surface, the rate-determining step is CO insertion. For hydrogenation to ethane, the reaction rate is determined by the replacement of CO with H. Considering the overall activation energy, we propose that on Rh(111), the hydroformylation reaction is preferred at low temperatures because it had a lower activation energy (0.91 eV) than hydrogenation (1.38 eV). However, the hydrogenation reaction will become dominant at higher temperatures due to the high activation energy. The energy barrier of the rate-determining step of hydroformylation was slightly decreased by doping Co, from 0.91 eV on Rh(111) to 0.85 eV on RhCo(111). In contrast, the overall activation energy of hydrogenation increased from 1.38 to 1.49 eV. Compared with the catalytic evaluation results, the DFT calculations predicted consistent results that the addition of Co to Rh decreased the  $E_a$  for hydroformylation reaction but increased the  $E_a$  for hydrogenation. Because the DFT calculations use the assumptions of 0 K, vacuum, and a simplified surface, they only predict the trend of adsorption energy and the activation barrier on different surfaces. The gap between the real catalyst in experiments and the model surface in DFT calculations makes the direct comparison unfeasible. Nevertheless, the DFT calculations successfully reveal the promotion effect of Co on Rh by predicting the change in the activation barrier due to the addition of Co in this work.

Based on the rate-determining steps for the two pathways, the selectivity change of hydroformylation can be predicted by

the energy difference between (IS4-IS2) and (TS2-IS2). We define  $\delta E$  as the difference between  $E(\text{IS4-IS2})$  and  $E(\text{TS2-IS2})$ . When comparing different catalyst surfaces, larger  $\delta E$  indicates that hydroformylation is preferred; that is, a higher selectivity to oxygenates will be obtained. For the two surfaces compared currently, with the addition of Co to Rh,  $\delta E$  increased from 0.47 to 0.64 eV (Figure 6 and Table S4), indicating that the surface electron environment was affected by a Rh-Co synergistic effect and the selectivity for hydroformylation was enhanced.

In the previous works, several studies had focused on the relevance between CO adsorption and hydroformylation selectivity. Yamagishi *et al.* suggested that the hydroformylation reaction was promoted by strongly adsorbed CO on the surface.<sup>33</sup> However, excessively strong interaction between CO and the catalyst surface was disadvantageous from other reports. Ro *et al.* studied the supported single atomic Rh/Al<sub>2</sub>O<sub>3</sub> catalyst modified by ReO<sub>x</sub> species.<sup>26</sup> They claimed that the introduction of ReO<sub>x</sub> decreased the CO binding energy, which was beneficial to form the free active site of Rh(CO<sup>\*</sup>)<sup>(\*)</sup> species in the insertion step but increased the active barrier for CO insertion. Tan *et al.* studied a Rh/AC catalyst treated by HNO<sub>3</sub> at different temperatures in a liquid reaction system<sup>8</sup> and found that strongly adsorbed CO was difficult to desorb and led to hydrogenation reaction, and medium strength adsorption of CO was favored for insertion.

In the current research, based on the experimental analysis and DFT calculations, we proposed that adsorbed CO with middle strength was better for ethene hydroformylation on Co modified Rh/SiO<sub>2</sub>. The DFT calculations indicate that the hydroformylation selectivity is determined by  $\delta E$ , which represents the energy difference between H replacement and CO migration. Excessively weak CO binding strength means easy replacement of CO but too strong adsorption suppresses both reactions. Therefore, both weakly and strongly adsorbed CO are not suitable for hydroformylation. Based on the *in situ* DRIFTS study, we showed that weakly adsorbed CO was easy to be replaced and resulted in hydrogenation. By further comparing the CO-TPD profiles with catalytic evaluation results, it can be concluded that strongly adsorbed CO was unfavorable for hydroformylation. Therefore, medium adsorption strength of CO was desired for better catalytic performance of hydroformylation, which is consistent with the DFT calculation results.

#### 4. CONCLUSIONS

The promotion effect of Co on the Rh-based catalyst for ethene hydroformylation was studied. The Rh-Co bimetallic catalysts were more active and selective than Rh/SiO<sub>2</sub> and Co/SiO<sub>2</sub> monometallic catalysts. The amount of exposed active sites was increased by Co addition, which enhanced the activity of the RhCo/SiO<sub>2</sub> bimetallic catalysts in hydroformylation. The interaction between Co and Rh was confirmed by H<sub>2</sub>-TPR, and this interaction affected the adsorption modes of CO on the catalyst surface. Based on the experimental and theoretical results, a mechanism was proposed for the promotion by Co on the activity and selectivity of hydroformylation. The selectivity was determined by the difference between CO migration and H replacement. The weakened Rh-CO bond of adsorbed CO on RhCo/SiO<sub>2</sub> favors the migration of CO for the CO insertion step and enhances hydroformylation, but the extremely weak adsorbed CO on Rh/SiO<sub>2</sub> is easily replaced by H and causes hydrogenation.

#### ASSOCIATED CONTENT

##### SI Supporting Information

The Supporting Information is available free of charge at <https://pubs.acs.org/doi/10.1021/acs.iecr.0c03437>.

DRIFTS of CO desorption; TOF comparison between Rh/SiO<sub>2</sub> and 0.4-RhCo/SiO<sub>2</sub>; catalyst stability and CO/H<sub>2</sub> ratio influence on 0.4-RhCo/SiO<sub>2</sub>; ruling out the external diffusion limitation; top view and side view of Rh(111) and RhCo(111); influence of slab thickness; IS, TS, and FS of the hydroformylation reactions; physical properties of 0.6Rh/SiO<sub>2</sub>, 0.6Rh0.23Co/SiO<sub>2</sub>, and 1Co/SiO<sub>2</sub>; activation energy comparing with literatures; comparison of catalyst performances with literatures; and energy values of reaction states (PDF)

#### AUTHOR INFORMATION

##### Corresponding Author

Tiefeng Wang — Beijing Key Laboratory of Green Reaction Engineering and Technology, Department of Chemical Engineering, Tsinghua University, Beijing 100084, China;  
 [orcid.org/0000-0002-4607-8650](https://orcid.org/0000-0002-4607-8650); Phone: 86-10-62794136; Email: [wangtf@tsinghua.edu.cn](mailto:wangtf@tsinghua.edu.cn); Fax: 86-10-62772051

##### Authors

Ning Huang — Beijing Key Laboratory of Green Reaction Engineering and Technology, Department of Chemical Engineering, Tsinghua University, Beijing 100084, China

Boyang Liu — Beijing Key Laboratory of Green Reaction Engineering and Technology, Department of Chemical Engineering, Tsinghua University, Beijing 100084, China

Xiaocheng Lan — Beijing Key Laboratory of Green Reaction Engineering and Technology, Department of Chemical Engineering, Tsinghua University, Beijing 100084, China

Complete contact information is available at:  
<https://pubs.acs.org/10.1021/acs.iecr.0c03437>

##### Notes

The authors declare no competing financial interest.

#### ACKNOWLEDGMENTS

The authors thank the financial support from the National Natural Science Foundation of China (no. 21676155) and the assistance on DFT calculation supported by the Tsinghua National Laboratory for Information Science and Technology. The authors also thank Prof. Dezheng Wang for his valuable discussion and comments.

#### REFERENCES

- (1) Li, C.; Wang, W.; Yan, L.; Ding, Y. A Mini Review on Strategies for Heterogenization of Rhodium-Based Hydroformylation Catalysts. *Front. Chem. Eng.* **2018**, *12*, 113–123.
- (2) Weiß, A.; Giese, M.; Lijewski, M.; Franke, R.; Wasserscheid, P.; Haumann, M. Modification of Nitrogen Doped Carbon for SILP Catalyzed Hydroformylation of Ethylene. *Catal. Sci. Technol.* **2017**, *7*, 5562–5571.
- (3) Franke, R.; Selent, D.; Börner, A. Applied Hydroformylation. *Chem. Rev.* **2012**, *112*, 5675–5732.
- (4) Navidi, N.; Thybaut, J. W.; Marin, G. B. Experimental Investigation of Ethylene Hydroformylation to Propanal on Rh and Co Based Catalysts. *Appl. Catal., A* **2014**, *469*, 357–366.
- (5) Tan, R.; Zheng, X.; Qu, B.; Sader, C. A.; Fandrick, K. R.; Senanayake, C. H.; Zhang, X. Tunable P-Chiral Bisdihydrobenzoox-

- aphosphole Ligands for Enantioselective Hydroformylation. *Org. Lett.* **2016**, *18*, 3346–3349.
- (6) Clark, T. P.; Landis, C. R.; Freed, S. L.; Klosin, J.; Abboud, K. A. Highly Active, Regioselective, and Enantioselective Hydroformylation with Rh. *J. Am. Chem. Soc.* **2005**, *127*, 5040–5042.
- (7) Jiao, Y.; Torne, M. S.; Gracia, J.; Niemantsverdriet, J. W.; van Leeuwen, P. W. N. M. Ligand Effects in Rhodium-Catalyzed Hydroformylation with Bisphosphines: Steric or Electronic? *Catal. Sci. Technol.* **2017**, *7*, 1404–1414.
- (8) Tan, M.; Wang, D.; Ai, P.; Liu, G.; Wu, M.; Zheng, J.; Yang, G.; Yoneyama, Y.; Tsubaki, N. Enhancing Catalytic Performance of Activated Carbon Supported Rh Catalyst on Heterogeneous Hydroformylation of 1-Hexene via Introducing Surface Oxygen-Containing Groups. *Appl. Catal., A* **2016**, *527*, 53–59.
- (9) Gorbunov, D.; Safranova, D.; Kardasheva, Y.; Maximov, A.; Rosenberg, E.; Karakhanov, E. New Heterogeneous Rh-Containing Catalysts Immobilized on a Hybrid Organic-Inorganic Surface for Hydroformylation of Unsaturated Compounds. *ACS Appl. Mater. Interfaces* **2018**, *10*, 26566–26575.
- (10) Kaftan, A.; Schönweiz, A.; Nikiforidis, I.; Hieringer, W.; Dyballa, K. M.; Franke, R.; Görting, A.; Libuda, J.; Wasserscheid, P.; Laurin, M.; Haumann, M. Supported Homogeneous Catalyst Makes its Own Liquid Phase. *J. Catal.* **2015**, *321*, 32–38.
- (11) Adint, T. T.; Landis, C. R. Immobilized Bis diazaphospholane Catalysts for Asymmetric Hydroformylation. *J. Am. Chem. Soc.* **2014**, *136*, 7943–7953.
- (12) Sun, Q.; Dai, Z.; Liu, X.; Sheng, N.; Deng, F.; Meng, X.; Xiao, F.-S. Highly Efficient Heterogeneous Hydroformylation over Rh-Metalated Porous Organic Polymers: Synergistic Effect of High Ligand Concentration and Flexible Framework. *J. Am. Chem. Soc.* **2015**, *137*, 5204–5209.
- (13) Li, C.; Xiong, K.; Yan, L.; Jiang, M.; Song, X.; Wang, T.; Chen, X.; Zhan, Z.; Ding, Y. Designing Highly Efficient Rh/CPOL-bp&PPh<sub>3</sub> Heterogenous Catalysts for Hydroformylation of Internal and Terminal Olefins. *Catal. Sci. Technol.* **2016**, *6*, 2143–2149.
- (14) Li, C.; Yan, L.; Lu, L.; Xiong, K.; Wang, W.; Jiang, M.; Liu, J.; Song, X.; Zhan, Z.; Jiang, Z.; Ding, Y. Single Atom Dispersed Rh-Biphepos&PPh<sub>3</sub>@Porous Organic Copolymers: Highly Efficient Catalysts for Continuous Fixed-Bed Hydroformylation of Propene. *Green Chem.* **2016**, *18*, 2995–3005.
- (15) Li, C.; Sun, K.; Wang, W.; Yan, L.; Sun, X.; Wang, Y.; Xiong, K.; Zhan, Z.; Jiang, Z.; Ding, Y. Xantphos Doped Rh/POPs-PPh<sub>3</sub> Catalyst for Highly Selective Long-Chain Olefins Hydroformylation: Chemical and DFT Insights into Rh Location and the Roles of Xantphos and PPh<sub>3</sub>. *J. Catal.* **2017**, *353*, 123–132.
- (16) Wang, Y.; Yan, L.; Li, C.; Jiang, M.; Zhao, Z.; Hou, G.; Ding, Y. Heterogeneous Rh/CPOL-BP&P(OPh)<sub>3</sub> Catalysts for Hydroformylation of 1-Butene: The Formation and Evolution of the Active Species. *J. Catal.* **2018**, *368*, 197–206.
- (17) Jia, X.; Liang, Z.; Chen, J.; Lv, J.; Zhang, K.; Gao, M.; Zong, L.; Xie, C. Porous Organic Polymer Supported Rhodium as a Reusable Heterogeneous Catalyst for Hydroformylation of Olefins. *Org. Lett.* **2019**, *21*, 2147–2150.
- (18) Marinkovic, J. M.; Riisager, A.; Franke, R.; Wasserscheid, P.; Haumann, M. Fifteen Years of Supported Ionic Liquid Phase-Catalyzed Hydroformylation: Material and Process Developments. *Ind. Eng. Chem. Res.* **2019**, *58*, 2409–2420.
- (19) Wei, M.; Zhang, X.; Evans, D. G.; Duan, X.; Li, X.; Chen, H. Rh-TPPTS Intercalated Layered Double Hydroxides as Hydroformylation Catalyst. *AIChE J.* **2007**, *53*, 2916–2924.
- (20) Matsinha, L. C.; Siangwata, S.; Smith, G. S.; Makhubela, B. C. E. Aqueous Biphasic Hydroformylation of Olefins: From Classical Phosphine-Containing Systems to Emerging Strategies Based On Water-Soluble Nonphosphine Ligands. *Catal. Rev.: Sci. Eng.* **2018**, *61*, 111–133.
- (21) Pogrzeba, T.; Müller, D.; Hamerla, T.; Esche, E.; Paul, N.; Wozny, G.; Schomäcker, R. Rhodium-Catalyzed Hydroformylation of Long-Chain Olefins in Aqueous Multiphase Systems in a Continuously Operated Miniplant. *Ind. Eng. Chem. Res.* **2015**, *54*, 11953–11960.
- (22) Coufourier, S.; Gaillard, S.; Clet, G.; Serre, C.; Daturi, M.; Renaud, J.-L. A MOF-Assisted Phosphine Free Bifunctional Iron Complex for the Hydrogenation of Carbon Dioxide, Sodium Bicarbonate and Carbonate to Formate. *Chem. Commun.* **2019**, *55*, 4977–4980.
- (23) Gadge, S. T.; Bhanage, B. M. Recent Developments in Palladium Catalysed Carbonylation Reactions. *RSC Adv.* **2014**, *4*, 10367–10389.
- (24) Tan, M.; Yang, G.; Wang, T.; Vitidsant, T.; Li, J.; Wei, Q.; Ai, P.; Wu, M.; Zheng, J.; Tsubaki, N. Active and Regioselective Rhodium Catalyst Supported on Reduced Graphene Oxide for 1-Hexene Hydroformylation. *Catal. Sci. Technol.* **2016**, *6*, 1162–1172.
- (25) Alvarado Rupflin, L.; Mormul, J.; Lejkowski, M.; Titlbach, S.; Papp, R.; Gläser, R.; Dimitrakopoulou, M.; Huang, X.; Trunschke, A.; Willinger, M. G.; Schlögl, R.; Rosowski, F.; Schunk, S. A. Platinum Group Metal Phosphides as Heterogeneous Catalysts for the Gas-Phase Hydroformylation of Small Olefins. *ACS Catal.* **2017**, *7*, 3584–3590.
- (26) Ro, I.; Xu, M.; Graham, G. W.; Pan, X.; Christopher, P. Synthesis of Heteroatom Rh-ReO<sub>x</sub> Atomically Dispersed Species on Al<sub>2</sub>O<sub>3</sub> and Their Tunable Catalytic Reactivity in Ethylene Hydroformylation. *ACS Catal.* **2019**, *9*, 10899–10912.
- (27) Zhang, J.; Sun, P.; Gao, G.; Wang, J.; Zhao, Z.; Muhammad, Y.; Li, F. Enhancing Regioselectivity via Tuning the Microenvironment In Heterogeneous Hydroformylation of Olefins. *J. Catal.* **2020**, *387*, 196–206.
- (28) Lang, R.; Li, T.; Matsumura, D.; Miao, S.; Ren, Y.; Cui, Y.-T.; Tan, Y.; Qiao, B.; Li, L.; Wang, A.; Wang, X.; Zhang, T. Hydroformylation of Olefins by a Rhodium Single-Atom Catalyst with Activity Comparable to RhCl(PPh<sub>3</sub>)<sub>3</sub>. *Angew. Chem., Int. Ed.* **2016**, *55*, 16054–16058.
- (29) Amsler, J.; Sarma, B. B.; Agostini, G.; Prieto, G.; Plessow, P. N.; Studt, F. Prospects of Heterogeneous Hydroformylation with Supported Single Atom Catalysts. *J. Am. Chem. Soc.* **2020**, *142*, 5087–5096.
- (30) Li, T.; Chen, F.; Lang, R.; Wang, H.; Su, Y.; Qiao, B.; Wang, A.; Zhang, T. Styrene Hydroformylation with *In Situ* Hydrogen: Regioselectivity Control by Coupling with the Low-Temperature Water-Gas Shift Reaction. *Angew. Chem., Int. Ed.* **2020**, *59*, 7430–7434.
- (31) Wang, L.; Zhang, W.; Wang, S.; Gao, Z.; Luo, Z.; Wang, X.; Zeng, R.; Li, A.; Li, H.; Wang, M.; Zheng, X.; Zhu, J.; Zhang, W.; Ma, C.; Si, R.; Zeng, J. Atomic-Level Insights in Optimizing Reaction Paths for Hydroformylation Reaction Over Rh/CoO Single-Atom Catalyst. *Nat. Commun.* **2016**, *7*, 14036.
- (32) Tomishige, K.; Furikado, I.; Yamagishi, T.; Ito, S.-i.; Kunimori, K. Promoting Effect of Mo on Alcohol Formation in Hydroformylation of Propylene and Ethylene on Mo-Rh/SiO<sub>2</sub>. *Catal. Lett.* **2005**, *103*, 15–21.
- (33) Yamagishi, T.; Furikado, I.; Ito, S.-i.; Miyao, T.; Naito, S.; Tomishige, K.; Kunimori, K. Catalytic Performance and Characterization of RhVO<sub>4</sub>/SiO<sub>2</sub> for Hydroformylation and CO Hydrogenation. *J. Mol. Catal. A: Chem.* **2006**, *244*, 201–212.
- (34) Sordelli, L. Characterization and Catalytic Performances of Alkali-Metal Promoted Rh/SiO<sub>2</sub> Catalysts for Propene Hydroformylation. *J. Mol. Catal. A: Chem.* **2003**, *204–205*, 509–518.
- (35) Ma, Y.; Fu, J.; Gao, Z.; Zhang, L.; Li, C.; Wang, T. Dicyclopentadiene Hydroformylation to Value-Added Fine Chemicals over Magnetically Separable Fe<sub>3</sub>O<sub>4</sub>-Supported Co-Rh Bimetallic Catalysts: Effects of Cobalt Loading. *Catalysts* **2017**, *7*, 103–112.
- (36) Huang, L.; Xu, Y. Promoting Effect of Doped Cobalt on catalysis of SiO<sub>2</sub>-Supported Rhodium for Propylene Hydroformylation. *React. Kinet. Catal. Lett.* **1997**, *61*, 397–404.
- (37) Kresse, G.; Furthmüller, J. Efficient Iterative Schemes for Ab Initio Total-Energy Calculations Using a Plane-Wave Basis Set. *Phys. Rev. B: Condens. Matter Mater. Phys.* **1996**, *54*, 11169–11186.

- (38) Kresse, G.; Furthmüller, J. Efficiency of Ab-Initio Total Energy Calculations for Metals and Semiconductors Using a Plane-Wave Basis Set. *Comput. Mater. Sci.* **1996**, *6*, 15–50.
- (39) Perdew, J. P.; Burke, K.; Ernzerhof, M. Generalized Gradient Approximation Made Simple. *Phys. Rev. Lett.* **1996**, *77*, 3865–3868.
- (40) Henkelman, G.; Überuaga, B. P.; Jónsson, H. A Climbing Image Nudged Elastic Band Method for Finding Saddle Points and Minimum Energy Paths. *J. Chem. Phys.* **2000**, *113*, 9901–9904.
- (41) Henkelman, G.; Jónsson, H. A Dimer Method for Finding Saddle Points On High Dimensional Potential Surfaces Using Only First Derivatives. *J. Chem. Phys.* **1999**, *111*, 7010–7022.
- (42) Olsen, R. A.; Kroes, G. J.; Henkelman, G.; Arnaldsson, A.; Jónsson, H. Comparison of Methods for Finding Saddle Points Without Knowledge of the Final States. *J. Chem. Phys.* **2004**, *121*, 9776–9792.
- (43) Kästner, J.; Sherwood, P. Superlinearly Converging Dimer Method for Transition State Search. *J. Chem. Phys.* **2008**, *128*, 014106.
- (44) Boukha, Z.; Gil-Calvo, M.; de Rivas, B.; González-Velasco, J. R.; Gutiérrez-Ortíz, J. I.; López-Fonseca, R. Behaviour of Rh Supported on Hydroxyapatite Catalysts in Partial Oxidation and Steam Reforming of Methane: On the Role of The Speciation of the Rh Particles. *Appl. Catal., A* **2018**, *556*, 191–203.
- (45) Ferencz, Z.; Erdőhelyi, A.; Baán, K.; Oszkó, A.; Óvári, L.; Kónya, Z.; Papp, C.; Steinrück, H.-P.; Kiss, J. Effects of Support and Rh Additive on Co-Based Catalysts in the Ethanol Steam Reforming Reaction. *ACS Catal.* **2014**, *4*, 1205–1218.
- (46) Li, X.; Wan, W.; Kattel, S.; Chen, J. G.; Wang, T. Selective Hydrogenation of Biomass-Derived 2(SH)-Furanone over Pt-Ni and Pt-Co Bimetallic Catalysts: From Model Surfaces to Supported Catalysts. *J. Catal.* **2016**, *344*, 148–156.
- (47) Kondarides, D. I.; Zhang, Z.; Verykios, X. E. Chlorine-Induced Alterations in Oxidation State and CO Chemisorptive Properties of CeO<sub>2</sub>-Supported Rh Catalysts. *J. Catal.* **1998**, *176*, 536–544.
- (48) Zhao, L.; Mu, X.; Liu, T.; Fang, K. Bimetallic Ni–Co catalysts Supported on Mn–Al Oxide for Selective Catalytic CO Hydrogenation to Higher Alcohols. *Catal. Sci. Technol.* **2018**, *8*, 2066–2076.
- (49) Hertrich, M. F.; Scharnagl, F. K.; Pews-Davtyan, A.; Kreyenschulte, C. R.; Lund, H.; Bartling, S.; Jackstell, R.; Beller, M. Supported Cobalt Nanoparticles for Hydroformylation Reactions. *Chemistry* **2019**, *25*, 5534–5538.
- (50) Brezny, A. C.; Landis, C. R. Recent Developments in the Scope, Practicality, and Mechanistic Understanding of Enantioselective Hydroformylation. *Acc. Chem. Res.* **2018**, *51*, 2344–2354.
- (51) Heard, C. J.; Hu, C.; Skoglundh, M.; Creaser, D.; Grönbeck, H. Kinetic Regimes in Ethylene Hydrogenation over Transition-Metal Surfaces. *ACS Catal.* **2016**, *6*, 3277–3286.
- (52) Heard, C. J.; Siahrostami, S.; Grönbeck, H. Structural and Energetic Trends of Ethylene Hydrogenation over Transition Metal Surfaces. *J. Phys. Chem. C* **2016**, *120*, 995–1003.